PAPER • OPEN ACCESS

Spin and polarization effects on the nonlinear Breit–Wheeler pair production in laser-plasma interaction

New Journal of Physics
The open access journal at the forefront of physics

Deutsche Physikalische Gesellschaft DPG
IOP Institute of Physics

Published in partnership with: Deutsche Physikalische Gesellschaft and the Institute of Physics

OPEN ACCESS

RECEIVED
10 February 2021

REVISED
9 June 2021

ACCEPTED FOR PUBLICATION
23 June 2021

PUBLISHED
15 July 2021

PAPER

Spin and polarization effects on the nonlinear Breit–Wheeler pair production in laser-plasma interaction

Huai-Hang Song[1,2], Wei-Min Wang[3,4,*], Yan-Fei Li[5], Bing-Jun Li[5], Yu-Tong Li[1,2,6,7,*], Zheng-Ming Sheng[4,8,9,10], Li-Ming Chen[4,8,10] and Jie Zhang[1,4,8]

[1] Beijing National Laboratory for Condensed Matter Physics, Institute of Physics, Chinese Academy of Sciences, Beijing 100190, People's Republic of China
[2] School of Physical Sciences, University of Chinese Academy of Sciences, Beijing 100049, People's Republic of China
[3] Department of Physics and Beijing Key Laboratory of Opto-Electronic Functional Materials and Micro-Nano Devices, Renmin University of China, Beijing 100872, People's Republic of China
[4] Collaborative Innovation Center of IFSA, Shanghai Jiao Tong University, Shanghai 200240, People's Republic of China
[5] Department of Nuclear Science and Technology, Xi'an Jiaotong University, Xi'an 710049, People's Republic of China
[6] CAS Center for Excellence in Ultra-Intense Laser Science, Shanghai 201800, People's Republic of China
[7] Songshan Lake Materials Laboratory, Dongguan, Guangdong 523808, People's Republic of China
[8] Key Laboratory for Laser Plasmas (MoE) and School of Physics and Astronomy, Shanghai Jiao Tong University, Shanghai 200240, People's Republic of China
[9] SUPA, Department of Physics, University of Strathclyde, Glasgow G4 0NG, United Kingdom
[10] Tsung-Dao Lee Institute, Shanghai Jiao Tong University, Shanghai 200240, People's Republic of China
[*] Authors to whom any correspondence should be addressed.

E-mail: weiminwang1@ruc.edu.cn and ytli@iphy.ac.cn

Keywords: spin and polarization effects, pair production, strong-field QED, laser-plasma interaction, particle-in-cell simulation

Abstract

The spin effect of electrons/positrons (e^-/e^+) and polarization effect of γ photons are investigated in the interaction of two counter-propagating linearly polarized laser pulses of peak intensity 8.9×10^{23} W cm^{-2} with a thin foil target. The processes of nonlinear Compton scattering and nonlinear Breit–Wheeler pair production based on the spin- and polarization-resolved probabilities are implemented into the particle-in-cell (PIC) algorithm by Monte Carlo methods. It is found from PIC simulations that the average degree of linear polarization of emitted γ photons can exceed 50%. This polarization effect leads to a reduced positron yield by about 10%. At some medium positron energies, the reduction can reach 20%. Furthermore, we also observe that the local spin polarization of e^-/e^+ leads to a slight decrease of the positron yield about 2% and some anomalous phenomena about the positron spectrum and photon polarization at the high-energy range, due to spin-dependent photon emissions. Our results indicate that spin and polarization effects should be considered in calculating the pair production and laser-plasma interaction with the laser power of 10 PW to 100 PW classes.

1. Introduction

Over the past decades, the intensity of lasers has increased rapidly [1, 2] with the laser technical progress based on chirped pulse amplification [3]. Several multi-petawatt (PW) [4] and 10 PW-class [5, 6] femtosecond laser systems have been built, which are expected to achieve an unprecedented peak power density up to the order of 10^{23-24} W cm^{-2} with tightly focusing. Such ultraintense lasers enable laser-plasma interactions to enter the quantum electrodynamics (QED) regime [7–9]. Electrons experiencing the ultraintense transverse field can stochastically radiate γ photons by nonlinear Compton scattering and lose a considerable amount of energy if the quantum parameter $\chi_e = (|e|\hbar/m_e^3c^4)|F_{\mu\nu}p^\nu| \gtrsim 1$ [10–12], where $F_{\mu\nu}$ is the field tensor, p^ν is the electron four-momentum, and the constants $\hbar$, m_e, e and c are the reduced Planck constant, the electron mass and charge, and the speed of light, respectively. As another cross channel of the same reaction, γ photons traveling through the ultraintense field possibly further decay into electron–positron (e^-e^+) pairs by nonlinear Breit–Wheeler process [13] with another

characteristic parameter $\chi_\gamma = (|e|\hbar^2/m_e^3c^4)|F_{\mu\nu}k^\nu|$, where $\hbar k^\nu$ is the photon four-momentum. This sort of pair production by light-by-light scattering was first demonstrated by the famous SLAC E-144 experiment [14] in the 1990s, where only about one hundred positrons were detected due to the limitation of the laser intensity at that time. The laser pulse and electron beam collisions utilizing today's high-intensity laser facilities in all-optical setups are also studied recently [15, 16].

With upcoming 10 PW-class lasers [6], abundant e^-e^+ pairs can even be produced in laser-plasma interactions without the need to pre-accelerate electrons to GeV energies. When such an ultraintense laser irradiates plasmas, electrons would be accelerated to ultrarelativistic energies and deflected by laser or strong self-generated fields in plasmas to gain a Lorentz boosted field strength in the electron's rest frame to achieve $\chi_e \gtrsim 1$. Many theoretical proposals for producing dense e^-e^+ pairs or even avalanche-like cascades have been put forward, such as through the laser collision configuration seeded by electrons/positrons (e^-/e^+) [17–19] or plasmas [20], and directly laser-solid interactions [21–24]. Generating copious positrons or dense e^-e^+ plasmas in the laboratory is of great importance in astrophysics [25–27], nuclear physics [28], and materials science [29].

Moreover, the e^-e^+ spin effect and γ-photon polarization effect have aroused interest in the strong-field QED regime [30–32]. An ultrarelativistic electron beam is found to be transversely spin-polarized by a single-shot collision of an elliptically polarized laser pulse [33] or a two-color laser pulse [34, 35] due to hard γ photon emissions, analogous to the Sokolov–Ternov effect [36, 37] in the static magnetic field. Similar spin polarization processes for newly created e^-e^+ pairs are also investigated [38–40]. The general view is that constructing an asymmetric laser field is the key to realize spin-polarized electrons or positrons. The emitted γ photons could be polarized via nonlinear Compton scattering [41–43], whose polarization strongly depends on the initial spin of electrons [42]. It is found that only linearly polarized γ photons can be generated by unpolarized or transversely polarized electrons [30, 42].

A more sophisticated description for e^-e^+ pair production by taking into account the e^-e^+ spin and γ-photon polarization has been discussed [30, 44, 45], based on single-particle-model analyses or simulations. The photon polarization is shown to significantly reduce the pair yield by a factor of over 10% in the collision of an ultraintense laser pulse and an electron beam [44]. In the rotating electric fields, the growth rate of the e^-e^+ cascade is also found to be suppressed [45]. However, in the laser-plasma interaction, it still demands to be studied to what extent the e^-e^+ spin and γ-photon polarization impact on the positron yield.

In this paper, we study the e^-e^+ pair production in the laser-plasma interaction by taking into account the spin of e^-/e^+ and the polarization of γ photons. The spin- and polarization-resolved probabilities of nonlinear Compton scattering and nonlinear Breit–Wheeler pair production are both implemented into the widely employed QED particle-in-cell (PIC) algorithm, which can self-consistently capture the collective plasma dynamics and QED processes. Here, we focus on the pair production in the interaction of two counter-propagating linearly polarized laser pulses of the same frequency and intensity with a thin foil target. This is a particularly advantageous configuration under the near-term laser intensity for triggering the QED pair production, due to the formation of the linearly-polarized electromagnetic standing wave (EMSW) [19, 46]. Our simulation results show that the positron yield is reduced by about 10% with the spin and polarization effects included for laser pulses with peak intensity 8.9×10^{23} W cm^{-2}. This significant difference is primarily caused by the polarized intermediate γ photons with an average linear-polarization degree of more than 50%. In addition, we also observe a decrease of positron number by about 2% and some anomalous phenomena for high-energy particles due to local spin polarization of e^-/e^+. This work indicates that the previously widely adopted spin- and polarization-averaged probabilities implemented in QED-PIC codes cannot accurately calculate the positron yield in the laser-plasma interaction for lasers of 10 PW to 100 PW classes, and spin and polarization effects should be considered.

2. Theoretical model and simulation method

In order to determine the spin of electron after the photon emission and also the polarization of emitted γ photon, the spin- and polarization-resolved photon emission probability is employed, which is derived in the Baier–Katkov QED operator method [12, 40, 42],

$$\frac{\mathrm{d}^2 W_{\mathrm{rad}}}{\mathrm{d}u\,\mathrm{d}t} = \frac{C_{\mathrm{rad}}}{4}\left\{\frac{u^2-2u+2}{1-u}K_{2/3}(y) - \mathrm{Int}\,K_{1/3}(y) - uK_{1/3}(y)(\boldsymbol{S}_{\mathrm{i}}\cdot\boldsymbol{e}_2)\right.$$
$$\left. + \left[2K_{2/3}(y) - \mathrm{Int}\,K_{1/3}(y)\right](\boldsymbol{S}_{\mathrm{i}}\cdot\boldsymbol{S}_{\mathrm{f}}) - \frac{u}{1-u}K_{1/3}(y)(\boldsymbol{S}_{\mathrm{f}}\cdot\boldsymbol{e}_2)\right.$$

$$+\frac{u^2}{1-u}\left[K_{2/3}(y)-\mathrm{Int}\,K_{1/3}(y)\right](\boldsymbol{S}_\mathrm{i}\cdot\boldsymbol{e}_v)(\boldsymbol{S}_\mathrm{f}\cdot\boldsymbol{e}_v)$$
$$+\frac{u}{1-u}K_{1/3}(y)(\boldsymbol{S}_\mathrm{i}\cdot\boldsymbol{e}_1)\xi_1+\left[\frac{2u-u^2}{1-u}K_{2/3}(y)-u\,\mathrm{Int}\,K_{1/3}(y)\right](\boldsymbol{S}_\mathrm{i}\cdot\boldsymbol{e}_v)\xi_2$$
$$+\left[K_{2/3}(y)-\frac{u}{1-u}K_{1/3}(y)(\boldsymbol{S}_\mathrm{i}\cdot\boldsymbol{e}_2)\right]\xi_3\Bigg\}, \tag{1}$$

where $K_\nu(y)$ is the second-kind modified Bessel function of the order of ν, $\mathrm{Int}\,K_{1/3}(y)\equiv\int_y^\infty K_{1/3}(x)\mathrm{d}x$, $C_\mathrm{rad}=(\alpha m_\mathrm{e}^2c^4)/(\sqrt{3}\pi\hbar\varepsilon_\mathrm{e})$, $y=2u/[3(1-u)\chi_\mathrm{e}]$, $u=\varepsilon_\gamma/\varepsilon_\mathrm{e}$, ε_e is the electron energy before the photon emission, ε_γ is the emitted photon energy, and $\alpha\approx1/137$ is the fine structure constant. Variable $\boldsymbol{e}_v$ is the unit vector along the electron velocity, $\boldsymbol{e}_1$ is the unit vector along the electron transverse acceleration, and $\boldsymbol{e}_2=\boldsymbol{e}_v\times\boldsymbol{e}_1$. $\boldsymbol{S}_\mathrm{i}$ and $\boldsymbol{S}_\mathrm{f}$ are the spin vectors of an electron before and after the photon emission, respectively, with $|\boldsymbol{S}_\mathrm{i,f}|=1$. The photon polarization is represented by Stokes parameters $\boldsymbol{\xi}=(\xi_1,\xi_2,\xi_3)$ with $|\boldsymbol{\xi}|=1$, defined with respect to the basis vector $(\boldsymbol{e}_1,\boldsymbol{e}_2,\boldsymbol{e}_v)$. The case $\xi_1=\xi_2=0$, $\xi_3=+1(-1)$ means the photon is linearly polarized along $\boldsymbol{e}_1(\boldsymbol{e}_2)$, and the case $\xi_1=\xi_3=0$, $\xi_2=+1(-1)$ means the photon is right-hand (left-hand) circularly polarized with respect to $\boldsymbol{e}_v$. After averaging over $\boldsymbol{S}_\mathrm{i}$ and summing up over $\boldsymbol{S}_\mathrm{f}$ and $\boldsymbol{\xi}$, the widely employed spin- and polarization-averaged photon emission probability [18, 47] is obtained. The above description can also be applied to the positron by replacing electron quantities with positron ones.

We have ignored the correlation terms involving both $\boldsymbol{S}_\mathrm{f}$ and $\boldsymbol{\xi}$ in equation (1), because the final electron spin and photon polarization are calculated separately in our Monte-Carlo algorithm for efficiency [48]. In particular, $\boldsymbol{\xi}$-dependent terms are averaged in the calculation of $\boldsymbol{S}_\mathrm{f}$; similarly, $\boldsymbol{S}_\mathrm{f}$-dependent terms are averaged as calculating $\boldsymbol{\xi}$. The simulation results via this algorithm are consistent with that of calculating $\boldsymbol{S}_\mathrm{f}$ first and then using the obtained $\boldsymbol{S}_\mathrm{f}$ to determine $\boldsymbol{\xi}$ [40] (see the good agreement in appendix A), which can also be proved analytically in appendix B. The radiative spin polarization with complete three dimensional (3D) information are resolved via the method adopted in [40, 48]. If a photon is emitted in a short time interval Δt, the spin vector of electron flips along the direction parallel or antiparallel to the instantaneous spin quantization axis (SQA) chosen as $\boldsymbol{S}_\mathrm{R}^*/|\boldsymbol{S}_\mathrm{R}^*|$, where $\boldsymbol{S}_\mathrm{R}^*=\left[2K_{2/3}(y)-\mathrm{Int}\,K_{1/3}(y)\right]\boldsymbol{S}_i-\frac{u}{1-u}K_{1/3}(y)\boldsymbol{e}_2+\frac{u^2}{1-u}\left[K_{2/3}(y)-\mathrm{Int}\,K_{1/3}(y)\right](\boldsymbol{S}_i\cdot\boldsymbol{e}_v)\boldsymbol{e}_v$. When the photon emission is rejected, the spin vector should also flip [40, 48] with respect to another SQA chosen as $\boldsymbol{S}_\mathrm{NR}^*/|\boldsymbol{S}_\mathrm{NR}^*|$ due to the selection effect [48] originated from the third term $-uK_{1/3}(y)(\boldsymbol{S}_\mathrm{i}\cdot\boldsymbol{e}_2)$ of equation (1), where $\boldsymbol{S}_\mathrm{NR}^*=\boldsymbol{S}_\mathrm{i}\left\{1-C_\mathrm{rad}\Delta t\int_0^1\left[\frac{u^2-2u+2}{1-u}K_{2/3}(y)-\mathrm{Int}\,K_{1/3}(y)\right]\mathrm{d}u\right\}+\boldsymbol{e}_2C_\mathrm{rad}\Delta t\int_0^1uK_{1/3}(y)\mathrm{d}u$. Another Monte Carlo method [33] for determining $\boldsymbol{S}_\mathrm{f}$ does not require the no-emission flip by choosing a selected SQA, e.g. along $\boldsymbol{e}_v$ or $\boldsymbol{e}_2$, so that it cannot retain 3D spin information. Therefore, our employed method [40, 48] here is more applicable to the complex electromagnetic field environment in laser-plasma interactions. Meanwhile, the Stokes parameters of emitted photon $\boldsymbol{\xi}$ is set to be one of two pure states $\pm\boldsymbol{\xi}^*/|\boldsymbol{\xi}^*|$, where $\boldsymbol{\xi}^*=(\xi_1^*,\xi_2^*,\xi_3^*)$, $\xi_1^*=\frac{u}{1-u}K_{1/3}(y)(\boldsymbol{S}_\mathrm{i}\cdot\boldsymbol{e}_1)$, $\xi_2^*=\left[\frac{2u-u^2}{1-u}K_{2/3}(y)-u\,\mathrm{Int}\,K_{1/3}(y)\right](\boldsymbol{S}_\mathrm{i}\cdot\boldsymbol{e}_v)$, and $\xi_3^*=K_{2/3}(y)-\frac{u}{1-u}K_{1/3}(y)(\boldsymbol{S}_\mathrm{i}\cdot\boldsymbol{e}_2)$ [42]. For convenience, we define high-energy photons with $u/(1-u)>1$ and low-energy photons with $u/(1-u)\ll1$.

Utilizing the similar method, the probability of the pair production with the photon polarization included can be written as [12, 40],

$$\frac{\mathrm{d}^2W_\mathrm{pairs}}{\mathrm{d}\varepsilon_+\mathrm{d}t}=\frac{C_\mathrm{pairs}}{2}\Bigg\{\frac{\varepsilon_+^2+\varepsilon_-^2}{\varepsilon_+\varepsilon_-}K_{2/3}(y)+\mathrm{Int}\,K_{1/3}(y)-\xi_3'K_{2/3}(y)$$
$$-\xi_1'\frac{\varepsilon_\gamma}{\varepsilon_-}K_{1/3}(y)(\boldsymbol{S}_+\cdot\boldsymbol{e}_1')-\left(\frac{\varepsilon_\gamma}{\varepsilon_+}-\xi_3'\frac{\varepsilon_\gamma}{\varepsilon_-}\right)K_{1/3}(y)(\boldsymbol{S}_+\cdot\boldsymbol{e}_2')$$
$$+\xi_2'\left[\frac{\varepsilon_\gamma}{\varepsilon_+}\mathrm{Int}\,K_{1/3}(y)+\left(\frac{\varepsilon_+}{\varepsilon_-}-\frac{\varepsilon_-}{\varepsilon_+}\right)K_{2/3}(y)\right](\boldsymbol{S}_+\cdot\boldsymbol{e}_v')\Bigg\}, \tag{2}$$

where $C_\mathrm{pairs}=(\alpha m_\mathrm{e}^2c^4)/(\sqrt{3}\pi\hbar\varepsilon_\gamma^2)$, $y=2\varepsilon_\gamma^2/(3\chi_\gamma\varepsilon_+\varepsilon_-)$, ε_- and ε_+ are the energies of the produced electron and positron, respectively. $\boldsymbol{S}_+$ is the spin vector of newly produced positron. The third term $-\xi_3'K_{2/3}(y)$ of equation (2) accounts for the photon polarization effect on the pair production probability $\mathrm{d}^2W_\mathrm{pairs}/(\mathrm{d}\varepsilon_+\,\mathrm{d}t)$. It is apparent that if ξ_3' is a positive value, $\mathrm{d}^2W_\mathrm{pairs}/(\mathrm{d}\varepsilon_+\,\mathrm{d}t)$ is reduced and consequently the positron yield decreases. The decrease can be up to 30% for medium-energy positrons [44]. The Stokes parameters need to be transformed from the photon emission frame $(\boldsymbol{e}_1,\boldsymbol{e}_2,\boldsymbol{e}_v)$ to the pair production frame $(\boldsymbol{e}_1',\boldsymbol{e}_2',\boldsymbol{e}_v)$ to obtain a new set of Stokes parameters (ξ_1',ξ_2',ξ_3') that required in

equation (2), through the matrix rotation [49]

$$\begin{aligned}\xi_1' &= \xi_1\ \cos(2\theta) - \xi_3\ \sin(2\theta),\\ \xi_2' &= \xi_2,\\ \xi_3' &= \xi_1\ \sin(2\theta) + \xi_3\ \cos(2\theta),\end{aligned} \tag{3}$$

where $\boldsymbol{e}_1'$ is the unit vector along $\boldsymbol{E}+\boldsymbol{e}_v\times\boldsymbol{B}-\boldsymbol{e}_v\cdot(\boldsymbol{e}_v\cdot\boldsymbol{E})$, $\boldsymbol{e}_2'=\boldsymbol{e}_1'\times\boldsymbol{e}_v$, and θ is the angle between $\boldsymbol{e}_1$ and $\boldsymbol{e}_1'$. When a pair of electron and positron is newly produced, the spin vector $\boldsymbol{S}_+$ of the positron is set to be $\boldsymbol{S}_+^*/|\boldsymbol{S}_+^*|$ via the stochastic procedure [40], where $\boldsymbol{S}_+^*=-\xi_1'(\varepsilon_\gamma/\varepsilon_-)K_{1/3}(y)\boldsymbol{e}_1'-(\varepsilon_\gamma/\varepsilon_+-\xi_3'\varepsilon_\gamma/\varepsilon_-)K_{1/3}(y)\boldsymbol{e}_2'+\xi_2'\left[(\varepsilon_\gamma/\varepsilon_+)\mathrm{Int}\,K_{1/3}(y)+(\varepsilon_+/\varepsilon_--\varepsilon_-/\varepsilon_+)K_{2/3}(y)\right]\boldsymbol{e}_v'$. Similarly, the spin vector $\boldsymbol{S}_-$ of the electron can be calculated by exchanging ε_+ and ε_-, and simultaneously setting $\boldsymbol{e}_1'$ along $-[\boldsymbol{E}+\boldsymbol{e}_v\times\boldsymbol{B}-\boldsymbol{e}_v\cdot(\boldsymbol{e}_v\cdot\boldsymbol{E})]$. In our cases, the spin vectors of pairs at birth according to equation (2) have a relatively weak influence on the pair production in the considered linearly-polarized EMSW. Their initial spin information will be quickly erased in the process of radiative polarization due to the photon emission, and the symmetrical field oscillation between positive and negative cycles also weakens the effects of initial spin states.

The semiclassical formulas of photon emission probability of equation (1) and pair production probability of equation (2) are derived based on the locally-constant-field approximation [50, 51], which is justified at an ultraintense laser intensity of $a_0=|e|E_\mathrm{L}/m_\mathrm{e}c\omega_0\gg 1$, where ω_0 is the laser frequency. The stochastic photon emission by an electron or a positron and the pair production by a γ photon are calculated using the standard QED Monte-Carlo algorithm [47, 52–54] but with the spin- and polarization-resolved probabilities. The e^-e^+ dynamics in the external electromagnetic field are described by classical Newton–Lorentz equations, and their spin dynamics are calculated according to the Thomas–Bargmann–Michel–Telegdi equation [55, 56]. More detailed Monte-Carlo methods for numerically modeling of spin and polarization effects we employ can be found in references [40, 48].

3. Simulation results and analysis

3.1. Simulation setup

We implement the spin- and polarization-resolved probabilities of equations (1) and (2) into the two-dimensional (2D) version of QED-PIC code YUNIC [57] by Monte-Carlo methods as described in section 2, to self-consistently study the e^-e^+ spin and γ photon polarization effects on the pair production in the laser-plasma interaction. The standard QED modules have been benchmarked in [57], and other benchmarks about the spin and polarization modules are presented in appendix A. In the following simulations, we can artificially switch on or off these two modules to better identify their impacts by comparison. In our simulation setups, two counter-propagating laser pulses with the same profile of $a_\mathrm{L}=a_0\sin^2(\pi t/\tau_0)\times\exp(-r^2/\sigma_0^2)$ within $0<t\leqslant\tau_0$ are normally incident from the left and right boundaries, respectively, and they are both linearly polarized along the y axis, where $r=y-y_0$. We take the laser normalized peak intensity $a_0=800$ (peak intensity $I_0\approx 8.9\times10^{23}$ W cm^{-2}), spot size $\sigma_0=2\lambda_0$, pulse duration $\tau_0=10T_0$, and propagation axis $y_0=7.5\lambda_0$, where $\lambda_0=1$ μm is the laser wavelength, and $T_0=2\pi/\omega_0\approx 3.33$ fs is the laser period. The corresponding laser peak power is approximately 56 PW. A 1 μm-thickness fully ionized foil target, composed of electrons and carbon ions (C^{6+}), is initially placed in the laser overlapping center of $3.5\lambda_0<x<4.5\lambda_0$ with an electron density of $n_\mathrm{e}=50n_\mathrm{c}$, where $n_\mathrm{c}=m_\mathrm{e}\omega_0^2/4\pi e^2$ is the critical density. The computational domain has a size of $8\lambda_0\times15\lambda_0$ in $x\times y$ directions with 384×720 cells. Each cell contains 100 macro electrons and 16 macro carbon ions. Absorbing boundaries are used for both particles and fields in any direction.

In the first simulation case, labeled as case (i), both the spin and polarization effects are incorporated. As reference cases, we have also performed another three simulations under the same physical parameters as those in case (i) except that: in case (ii), the spin and polarization effects are not included, which is the widely adopted method in the current QED-PIC codes [47, 52, 54]; in case (iii), only the spin effect is included, where the polarization-dependent terms are summed up over in equation (1) and averaged over in equation (2), while retaining spin-dependent terms in these two probability equations; in case (iv), we switch off the photon annihilation and pair production processes but still include the spin and polarization effects, to check the original polarization characteristics of emitted γ photons.

3.2. Simulation results

For case (i), figure 1(a) illustrates the spatial distribution of the positron density n_+ at the end of the laser-foil interaction at $t=12T_0$ when two laser pulses have passed through each other. Dense and spatially

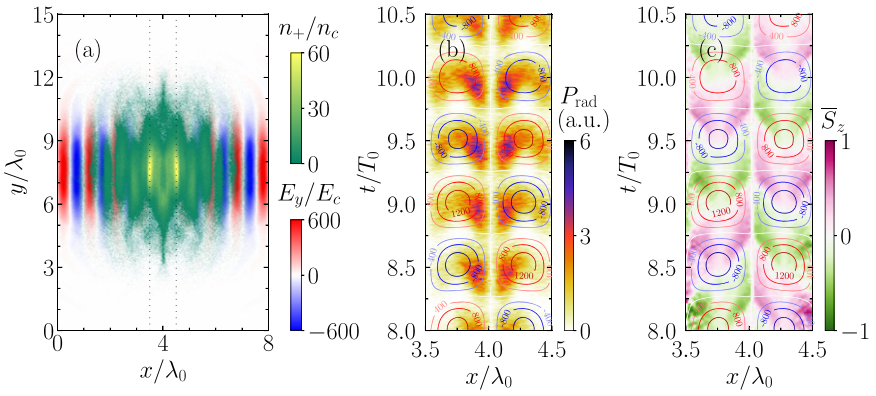

Figure 1. Simulation results of case (i). (a) Spatial distribution of the density of produced positrons n_+, together with the electric field E_y of two counter-propagating laser pulses at $t = 12T_0$, where E_c is $m_e\,c\omega_0/|e|$. The dotted lines outline the initial boundaries of the foil target. Space-time evolution of (b) the radiation power $P_{\rm rad}$ of photons with energies above 100 MeV and (c) the average electron spin $\overline{S}_z$ along $y = 7.5\lambda_0$. The laser magnetic field B_z normalized by $m_e\,c\omega_0/|e|$ is also shown by contour lines to outline the magnetic region of the EMSW both in (b) and (c).

modulated [58] positrons are produced, with a maximum density of $n_+ = 60n_c$, already exceeding the initial electron density of the foil target. A transient linearly-polarized EMSW responsible for the abundant positron production is constructed by two counter-propagating linearly polarized laser pulses in the time interval $7T_0 < t < 11T_0$, covering the entire foil plasma zone. The space-time evolution of magnetic field component B_z of EMSW along $y = 7.5\lambda_0$ is shown by contour lines both in figures 1(b) and (c). The formed EMSW is divided into electric region (maximize at magnetic nodes $x = m\lambda_0/2$ and $t = nT_0/2 + T_0/4$) and magnetic region (maximize at magnetic antinodes $x = m\lambda_0/2 + \lambda_0/4$ and $t = nT_0/2$), where m and n are integers. These two distinct regions are shifted by $\lambda_0/4$ spatially and $T_0/4$ temporally ($\pi/2$ phase offset). Furthermore, electrons are accelerated or decelerated by the electric field along the y direction in the electric region, while emitting photons and simultaneously losing energies primarily in the magnetic region [22]. The photon radiation power $P_{\rm rad}$ shown in figure 1(b) verifies that more high-energy photons are emitted in the early stage after entering the magnetic region. The previous study [46] has presented that this type of field configuration is favorable for improving quantum parameter χ_e at laser intensity $\sim 10^{23}$ W cm^{-2}, and consequently are the photon emission and pair production. In this simulation case, χ_e can reach a maximum of 3. At the end of the simulation, about 30% laser energies are absorbed, among which, 24% are transformed into photons, 5.5% into electrons and positrons, and less than 0.5% into ions.

The time evolution of the total positron number N_+ of cases (i)–(iii) is illustrated in figure 2(a). During the existence of EMSW in the time interval of $7T_0 < t < 11T_0$, N_+ increases dramatically. The stair-step-like growth with a period of $0.5T_0$ is attributed to the fact that electrons strongly emit photons mostly in magnetic regions as already shown in figure 1(b). The most important feature is that when the spin and polarization effects are fully considered in case (i), the total number of positrons is reduced by 12% compared with the case (ii) that excluding the two effects, i.e. $\Delta N_+^{\rm i-ii} = (N_+^{\rm i} - N_+^{\rm ii})/N_+^{\rm ii} \approx -12\%$. Furthermore, the relative deviation of positron energy spectrum $\delta N_+^{\rm i-ii}$ also depends on the positron energy ε_+ shown in figure 2(b), exhibiting a maximum difference as large as -20% at $\varepsilon_+ = 0.2$ GeV. The difference of positron yield is mainly attributed to the linear polarization of emitted γ photons, which will be detailed in the next subsection.

Then, we analyze the spin dynamics of electrons in the linearly-polarized EMSW. As emitting a high-energy photon, the electron spin more probably flips to the direction antiparallel to the magnetic field in the electron's rest frame, according to equation (1) (see figure 4(b) in reference [34]). In the magnetic region where photon emissions are concentrated, the spin-flip trend of electrons is determined by the direction of magnetic field B_z. More specifically, the electron spin is more likely antiparallel to the B_z direction after the photon emission (and positron spin is more likely parallel to that). This is evidenced by the time-space evolution of the average spin component $\overline{S}_z$ of electrons shown in figure 1(c), which characterizes their transverse spin polarization because electrons move almost perpendicularly to the z axis. It shows that $\overline{S}_z$ is temporally oscillating with a laser frequency ω_0. However, the total degree of spin remains nearly zero due to the symmetry between positive and negative cycles of the laser field, which is a kind of local spin polarization.

By comparing the total positron number N_+ of cases (ii) and (iii) in figure 2(a), one also notices that the positron yield is reduced by about 2.5% due to the pure spin effect. This reduction is caused by the local

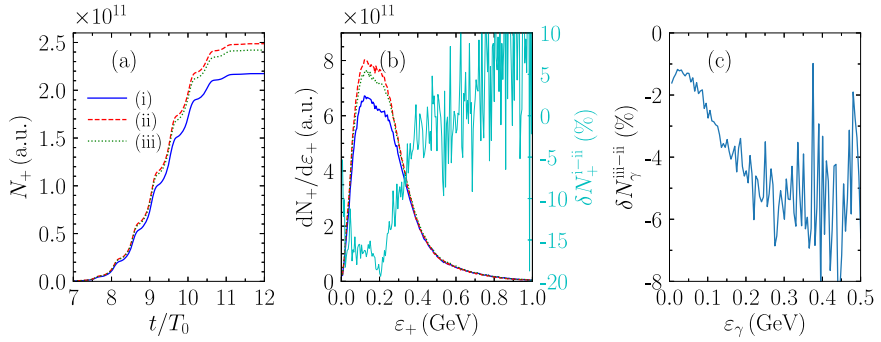

Figure 2. (a) The time evolution of total positron number N_+ in three simulation cases: case (i) with spin and polarization effects (blue solid line), case (ii) without spin and polarization effects (red dashed line), and case (iii) with only spin effect (green dotted line). (b) Positron energy spectrum $\mathrm{d}N_+/\mathrm{d}\varepsilon_+$ under the three cases at the end of the laser interaction. The relative deviation $\delta N_+^{\mathrm{i-ii}} = (\mathrm{d}N_+^{\mathrm{i}}/\mathrm{d}\varepsilon_+ - \mathrm{d}N_+^{\mathrm{ii}}/\mathrm{d}\varepsilon_+)/(\mathrm{d}N_+^{\mathrm{ii}}/\mathrm{d}\varepsilon_+)$ between cases (i) and (ii) is also presented by the cyan line. (c) The relative deviation $\delta N_\gamma^{\mathrm{iii-ii}} = (\mathrm{d}N_\gamma^{\mathrm{iii}}/\mathrm{d}\varepsilon_\gamma - \mathrm{d}N_\gamma^{\mathrm{ii}}/\mathrm{d}\varepsilon_\gamma)/(\mathrm{d}N_\gamma^{\mathrm{ii}}/\mathrm{d}\varepsilon_\gamma)$ of photon energy spectrum between cases (iii) and (ii).

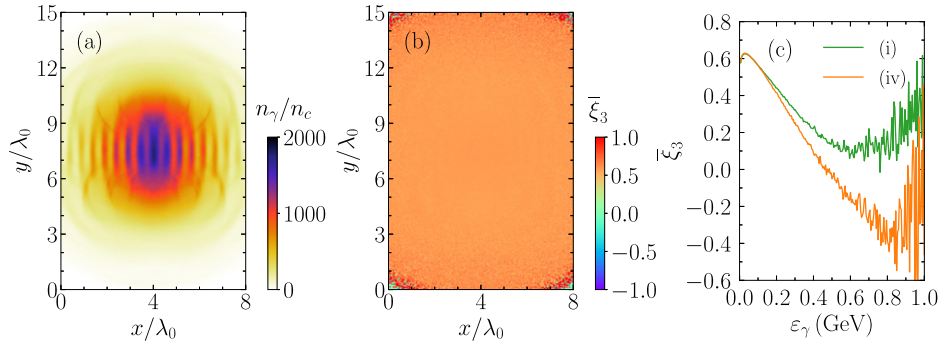

Figure 3. Spatial distribution of (a) photon density n_γ and (b) average photon polarization $\overline{\xi}_3$ at $t = 12T_0$ in case (i). (c) $\overline{\xi}_3$ versus photon energy ε_γ obtained from cases (i) and (iv), respectively, where we switch off the pair production module while include spin and polarization effects in case (iv).

spin polarization of electrons in the EMSW. When electrons just enter the magnetic region, their initial spins are mainly parallel to the direction of the magnetic field (spin-up, defined by $\boldsymbol{S}_{\mathrm{i}} \cdot \boldsymbol{e}_2 > 0$) (see figure 1(c)), owing to the radiative spin polarization in the previous magnetic region. The spin-dependent photon emission probability is therefore reduced, especially for high-energy photons [see the third term $-uK_{1/3}(y)(\boldsymbol{S}_{\mathrm{i}} \cdot \boldsymbol{e}_2)$ of equation (1) and figure 4(a) in reference [34]]. Then, the electron spin gradually flips to be antiparallel to the magnetic field direction (spin-down, defined by $\boldsymbol{S}_{\mathrm{i}} \cdot \boldsymbol{e}_2 < 0$). After entering the next magnetic region, the direction of the magnetic field B_z is reversed. The electron spin direction becomes parallel to the B_z direction again, and consequently the same process arises with slightly weaker photon emission. The relative deviation of photon energy spectrum $\delta N_\gamma^{\mathrm{iii-ii}}$ is plotted in figure 2(c). The absolute value of $\delta N_\gamma^{\mathrm{iii-ii}}$ increases with the increase of photon energy ε_γ for $\varepsilon_\gamma < 0.4$ GeV. These high-energy γ photons more likely decay into e^+e^- pairs, leading to a slightly smaller positron yield in figure 2(a). The spin effect discussed above is five times weaker than the photon polarization effect in terms of positron yield, and therefore we will mainly focus on the latter one. However, we note that the polarization of high-energy emitted photons highly relies on the spin of emitting electrons, hence the local spin polarization could have a prominent impact on the high-energy positron yield (see the next subsection).

3.3. Photon polarization properties

The remarkable difference of the positron yield between cases (i) and (ii) (see figures 2(a) and (b)) mostly originates in the highly linearly polarized γ photons. Figures 3(a) and (b) present spatial distributions of the photon density n_γ and average photon polarization $\overline{\xi}_3$ at $t = 12T_0$ in case (i), in which both spin and polarization effects are included. The other two polarization components $\overline{\xi}_1$ and $\overline{\xi}_2$ are nearly zero, so not shown here. $\overline{\xi}_3$ is rather uniform in space with a positive value of about 0.58, indicating that photons are emitted predominantly with a linear polarization along $\boldsymbol{e}_1$ at each photon emission frame, i.e. always in the x–y plane.

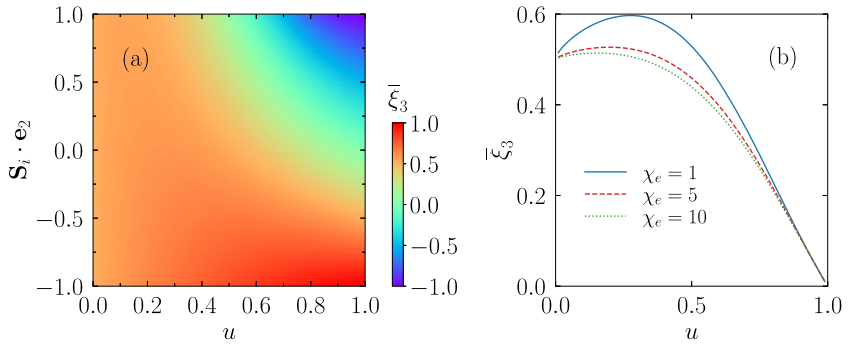

Figure 4. Theoretical calculations according to equation (4). (a) $\overline{\xi}_3$ versus emitted photon energy ratio $u = \varepsilon_\gamma/\varepsilon_e$ and the initial electron spin vector $\boldsymbol{S}_i \cdot \boldsymbol{e}_2$ for $\chi_e = 1$. (b) $\overline{\xi}_3$ versus u at $\boldsymbol{S}_i \cdot \boldsymbol{e}_2 = 0$ for $\chi_e = 1$, 5, and 10.

The spin- and polarization-resolved probabilities in equations (1) and (2) can be simplified in the interaction between the considered linearly-polarized EMSW and un-prepolarized electrons. It is appropriate to sum up over $\boldsymbol{S}_f$ terms, neglect $\boldsymbol{S}_i \cdot \boldsymbol{e}_1$ and $\boldsymbol{S}_i \cdot \boldsymbol{e}_v$ terms, but retain $\boldsymbol{S}_i \cdot \boldsymbol{e}_2$ terms in equation (1), since electrons are only spin-polarized along $\pm\boldsymbol{e}_2$ via the radiative polarization process, i.e. parallel or antiparallel to B_z direction. Therefore, the average Stokes parameters of emitted photons can be approximately as

$$\begin{aligned}
&\bar{\xi}_1 \approx 0,\\
&\bar{\xi}_2 \approx 0,\\
&\bar{\xi}_3 \approx \frac{1}{2}\frac{\mathrm{d}W_{\mathrm{rad}}^{\xi_3=+1} - \mathrm{d}W_{\mathrm{rad}}^{\xi_3=-1}}{\mathrm{d}W_{\mathrm{rad}}^{\xi_3=+1} + \mathrm{d}W_{\mathrm{rad}}^{\xi_3=-1}} = \frac{K_{2/3}(y) - \frac{u}{1-u}K_{1/3}(y)(\boldsymbol{S}_i \cdot \boldsymbol{e}_2)}{\frac{u^2-2u+2}{1-u}K_{2/3}(y) - \mathrm{Int}\,K_{1/3}(y) - uK_{1/3}(y)(\boldsymbol{S}_i \cdot \boldsymbol{e}_2)},
\end{aligned} \tag{4}$$

where

$$\begin{aligned}
\mathrm{d}W_{\mathrm{rad}}^{\xi_3=\pm1} = \frac{C_{\mathrm{rad}}}{2}\Bigg\{&\frac{u^2-2u+2}{1-u}K_{2/3}(y) - \mathrm{Int}\,K_{1/3}(y) - uK_{1/3}(y)(\boldsymbol{S}_i \cdot \boldsymbol{e}_2)\\
&\pm\left[K_{2/3}(y) - \frac{u}{1-u}K_{1/3}(y)(\boldsymbol{S}_i \cdot \boldsymbol{e}_2)\right]\Bigg\}.
\end{aligned} \tag{5}$$

Equation (4) indicates that the emitted photons cannot be circularly polarized since $\overline{\xi}_2 = 0$. Accordingly, the theoretical $\overline{\xi}_3$ as a function of u and $\boldsymbol{S}_i \cdot \boldsymbol{e}_2$ is shown in figure 4(a). For the low-energy photon, $\overline{\xi}_3$ is always positive with a value of about 0.5, insensitive to the initial spin vector $\boldsymbol{S}_i$ of the emitting electron. While for the high-energy photon, $\overline{\xi}_3$ strongly depends on $\boldsymbol{S}_i \cdot \boldsymbol{e}_2$. Spin-up electrons are prone to emit photons linearly polarized along $\boldsymbol{e}_2$ axis (z axis in our case) with $\overline{\xi}_3 < 0$; for spin-down electrons, one can obtain an opposite result of $\overline{\xi}_3 > 0$. In general, $\overline{\xi}_3$ value decreases with the increase of photon energy ε_γ. This trend is supported by the simulation curve for case (i) shown in figure 3(c), that $\overline{\xi}_3 \approx 0.5$ at $\varepsilon_\gamma = 0.1$ GeV and only $\overline{\xi}_3 \approx 0.1$ at $\varepsilon_\gamma = 0.6$ GeV.

The transformation of Stokes parameters from (ξ_1, ξ_2, ξ_3) to (ξ_1', ξ_2', ξ_3') can also be greatly simplified in our case with the linearly-polarized EMSW. One can obtain the transformation angle $\theta \approx 0$ or π for the fact that the acceleration direction and velocity direction of electrons are both well confined in the x–y plane (laser polarization plane). Consequently, ξ_3 with respect to the emission frame $(\boldsymbol{e}_1, \boldsymbol{e}_2, \boldsymbol{e}_v)$ can be directly substituted into equation (2), i.e. $\xi_3 \approx \xi_3'$. Hence, the positive values of ξ_3 directly leads to the reduction of the positron yield.

The photon polarization and positron yield at their higher energies exhibit some anomalous phenomena compared with those at their lower energy range, due to the local spin polarization of electrons. As outlined above, the most intense photon emissions occur in the early stage of each magnetic region, in which the spin-up emitting electrons dominate. The resulting decrease in the photon yield has been observed in figure 2(c). Besides the photon yield, the polarization of high-energy photons is also strongly affected by these locally spin-polarized electrons. Figure 3(c) for case (iv) indicates the original emitted photons with $\varepsilon_\gamma > 0.5$ GeV possess the negative $\overline{\xi}_3$. It is coincident with the theoretical analysis shown in figure 4(a) that spin-up electrons are in favor of emitting high-energy photons of negative-value $\overline{\xi}_3$. This eventually leads to an increase of positron yield at positron energies higher than 0.5 GeV, rather than decreasing like that at low energies in figure 2(b). Moreover, as we switch on the pair production process and include the γ-photon

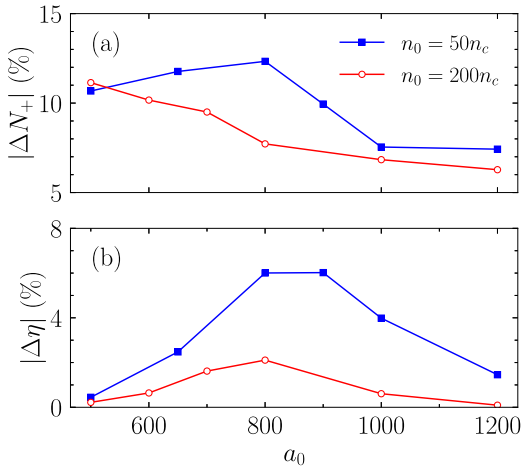

Figure 5. The absolute relative deviation of (a) positron number $|\Delta N_+| = |(N_+^{\rm i} - N_+^{\rm ii})/N_+^{\rm ii}|$ and (b) absorption fraction of laser energy $|\Delta\eta| = |(\eta^{\rm i} - \eta^{\rm ii})/\eta^{\rm ii}|$ between including and excluding spin and polarization effects, under various laser strengths $a_0 = 500$ to 1200 and initial plasma densities $n_0/n_c = 50$ and 200.

annihilation in case (i), the polarization $\overline{\xi}_3$ of high-energy photons increases as compared to those in case (iv), shown in figure 3(c). This can be explained by that photons of negative ξ_3 are easier to annihilate into e^-e^+ pairs, according to the polarization-dependent pair production probability of equation (2).

3.4. Impacts of laser intensity and plasma density

In figure 5(a), we investigate the difference of positron yield between with and without spin and polarization effects under various laser intensities a_0, to find the laser intensity at which these two effects need to be taken into account. For the case of initial plasma density $n_0 = 50n_c$, the absolute relative deviation $|\Delta N_+|$ of total positron number first slightly increases with a_0 and reaches a maximum 12% at $a_0 = 800$, then it gradually decreases to 7% at $a_0 = 1200$ ($I_0 \approx 2.0 \times 10^{24}$ W cm^{-2}). For a higher-density plasma of $n_0 = 200n_c$, $|\Delta N_+|$ always decreases with a_0 within the range of scanning parameters, i.e. decreasing from 11% at $a_0 = 500$ ($I_0 \approx 3.5 \times 10^{23}$ W cm^{-2}) to 6% at $a_0 = 1200$. On the whole, $|\Delta N_+|$ is larger in the case of $n_0 = 50n_c$ than that of $n_0 = 200n_c$ at the same a_0. These results can be basically explained according to figure 4(b), in which the average polarization $\overline{\xi}_3$ as a function of $u(\varepsilon_\gamma/\varepsilon_e)$ under three different quantum parameters χ_e is plotted according to equation (4). Here, we assume $\boldsymbol{S}_i \cdot \boldsymbol{e}_2 = 0$, which is approximately valid since electrons or positrons cannot gain a net degree of spin polarization in the linearly-polarized EMSW, and the influence of local spin polarization on the positron yield is smaller compared with the photon polarization one. From figure 4(b), $\overline{\xi}_3$ is smaller for a larger χ_e (corresponding to a larger a_0); hence a smaller difference between positron yields can be expected.

The decrease of generated e^-e^+ yield can result in a lowered laser absorption since less e^-/e^+ are accelerated in the laser field (absorb laser energy) and less γ photons are emitted. Figure 5(b) shows the spin and polarization effects on the absorption fraction of laser energy η as a function of laser intensity a_0. The absolute relative deviation $|\Delta\eta|$ can reach a maximum of 6% for $n_0 = 50n_c$ and 2% for $n_0 = 200n_c$, respectively. Above $a_0 = 800$, $|\Delta\eta|$ decreases with the increase of a_0, which is similar to $|\Delta N_+|$. Below $a_0 = 800$, $|\Delta\eta|$ also decreases as reducing a_0 and only $\Delta\eta < 0.5\%$ is observed at $a_0 = 500$, indicating that the spin and polarization effects have a negligible impact on the laser absorption below $a_0 = 500$, although the difference of positron yield is more obvious at relatively low laser intensities. This is because the pair production probability $\mathrm{d}^2W_{\rm pairs}/(\mathrm{d}\varepsilon_+\,\mathrm{d}t)$ of equation (2) is exponentially small for $\chi_\gamma \ll 1$, so that only a small number of positrons is produced. At $a_0 < 500$, the energy conversion efficiency from laser to positron is less than 1%, hence the impact of $|\Delta N_+|$ on $|\Delta\eta|$ can be neglected.

4. Conclusion

In conclusion, with e^-e^+ spin and γ-photon polarization effects implemented, we have investigated the pair production in the interaction of two counter-propagating laser pulses with a thin foil target via QED-PIC simulations. These two effects can lead to a decrease of total positron yield by about 10%, and the relative difference can even reach 20% for medium-energy positrons. The positron decrease mainly comes from up to 50% linear polarization of emitted γ photons. In addition, we also observe several anomalous phenomena about positron yield and photon polarization of high-energy particles caused by the local spin

polarization of e^-/e^+. Basically, the spin and polarization effects on the pair production become weaker with the increase of laser intensities from 3.5×10^{23} W cm^{-2} to 2.0×10^{24} W cm^{-2}. In terms of laser absorption, their impacts are strongest at a moderate intensity around 8.9×10^{23} W cm^{-2}, and weaker both at lower and higher laser intensities. Our results indicate that the spin- and polarization-averaged probabilities widely adopted in QED-PIC simulations overestimate the positron yield for laser pulses of 10 PW to 100 PW classes, and correspondingly lead to an overestimated laser absorption in the laser-plasma interaction.

Acknowledgments

This work was supported by the National Key R & D Program of China (Grant No. 2018YFA0404801), National Natural Science Foundation of China (Grant Nos. 11775302, 11721091, 11991073, and 12075187), the Strategic Priority Research Program of Chinese Academy of Sciences (Grant Nos. XDA25050300, XDA25010300, and XDB16010200), Science Challenge Project of China (Grant Nos. TZ2016005 and TZ2018005), and the Fundamental Research Funds for the Central Universities, the Research Funds of Renmin University of China (20XNLG01).

Data availability statement

All data that support the findings of this study are included within the article (and any supplementary files).

Appendix A. Spin and polarization benchmarks

We have performed two additional 2D QED-PIC simulations with the code YUNIC to benchmark against Monte-Carlo simulations in reference [40], where ultrarelativistic electrons with 1 GeV move along $+x$ axis in the x–y plane under a perpendicularly static external magnetic field of $B_0 = 100 m_e c\omega_0/|e|$. We take the computational domain of $8\lambda_0 \times 8\lambda_0$ in $x \times y$ directions with 128×128 cells, and 16 macro electrons per cell, where $\lambda_0 = 2\pi c/\omega_0 = 1$ μm. The electron density is low enough to avoid the influence of the self-generated electromagnetic field, and periodic boundaries are employed. Figures A1(a) and (b) show the time evolution of average spin vector $\overline{\boldsymbol{S}}$ of electrons and average Stokes parameters $\overline{\boldsymbol{\xi}}$ of emitted photons for the initially unpolarized electrons, respectively; figures A1(c) and (d) are those for initially longitudinally polarized electrons. Our QED-PIC simulations are in good agreement with Monte-Carlo simulations in reference [40].

Appendix B. Determination order of spin and polarization

Here, we prove that both the average spin vector of the electron $\overline{\boldsymbol{S}}_\mathrm{f}$ after the emission and the average Stokes parameters of the emitted photon $\overline{\boldsymbol{\xi}}$ in nonlinear Compton scattering by calculating $\boldsymbol{S}_\mathrm{f}$ first and then $\boldsymbol{\xi}$ are the same as those by calculating them separately. The complete spin- and polarization-resolved photon emission probability [12, 40, 42] can be written in the following form,

$$W_\mathrm{rad} = Q_0 + \boldsymbol{S}_\mathrm{f} \cdot \boldsymbol{Q}_1 + \boldsymbol{\xi} \cdot \boldsymbol{Q}_2 + Q_3(\boldsymbol{S}_\mathrm{f}, \boldsymbol{\xi}), \tag{B.1}$$

where Q_0, $\boldsymbol{Q}_1$, and $\boldsymbol{Q}_2$ are independent of $\boldsymbol{S}_\mathrm{f}$ and $\boldsymbol{\xi}$. $Q_3(\boldsymbol{S}_\mathrm{f}, \boldsymbol{\xi})$ is the correlation term involving both $\boldsymbol{S}_\mathrm{f}$ and $\boldsymbol{\xi}$, which is ignored in equation (1).

The spin vector of the electron $\boldsymbol{S}_\mathrm{f}$ after emitting a photon is chosen as $\pm\boldsymbol{Q}_1/|\boldsymbol{Q}_1|$, and their relative probabilities can be calculated from equation (B.1) by averaging $\boldsymbol{\xi}$-dependent terms:

$$P_+\left(\boldsymbol{S}_\mathrm{f} = \frac{\boldsymbol{Q}_1}{|\boldsymbol{Q}_1|}\right) = \frac{Q_0 + |\boldsymbol{Q}_1|}{2Q_0}, \tag{B.2}$$

$$P_-\left(\boldsymbol{S}_\mathrm{f} = -\frac{\boldsymbol{Q}_1}{|\boldsymbol{Q}_1|}\right) = \frac{Q_0 - |\boldsymbol{Q}_1|}{2Q_0}. \tag{B.3}$$

Therefore, the obtained average vector $\overline{\boldsymbol{S}}_\mathrm{f}$ is along

$$\overline{\boldsymbol{S}}_\mathrm{f}^* = \frac{\boldsymbol{Q}_1}{|\boldsymbol{Q}_1|}P_+ - \frac{\boldsymbol{Q}_1}{|\boldsymbol{Q}_1|}P_- = \frac{\boldsymbol{Q}_1}{Q_0}. \tag{B.4}$$

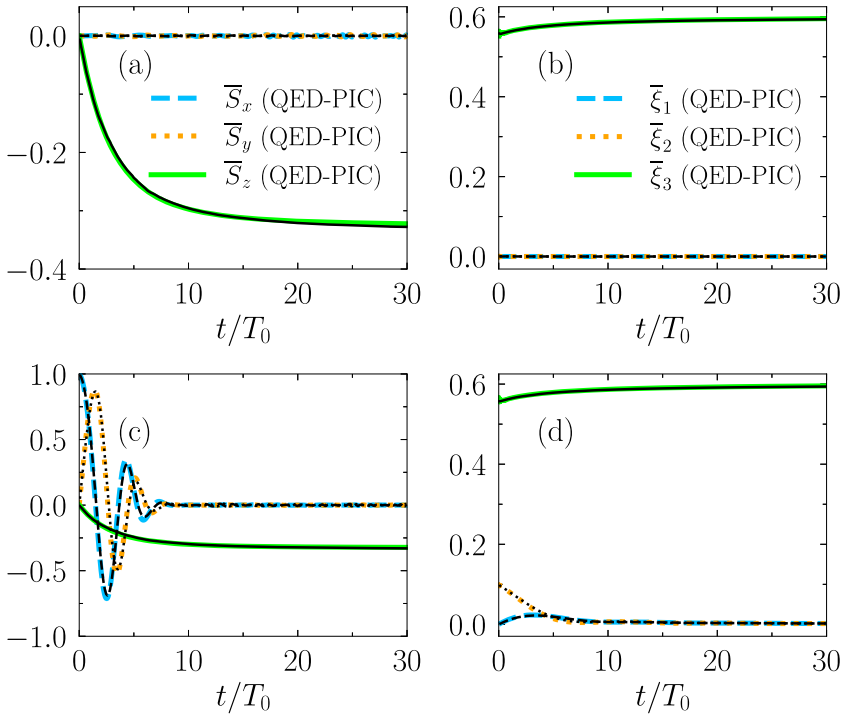

Figure A1. Comparison of our 2D QED-PIC simulations (thick colored lines) with Monte-Carlo simulations in reference [40] (thin black lines) in the radiative spin polarization of initially (a) and (b) unpolarized and (c) and (d) longitudinally polarized electrons, respectively. (a) and (c) Average spin vector of electrons $\overline{S}_x$, $\overline{S}_y$ and $\overline{S}_z$. (b) and (d) Average Stokes parameters of all emitted photons $\overline{\xi}_1$, $\overline{\xi}_2$ and $\overline{\xi}_3$ with respect to the emission frame.

After $\boldsymbol{S}_\mathrm{f}$ is determined, we proceed to determine $\boldsymbol{\xi}$ by inserting the obtained $\boldsymbol{S}_\mathrm{f}$ into equation (B.1), and note that $Q_3(\boldsymbol{S}_\mathrm{f},\boldsymbol{\xi}) = -Q_3(-\boldsymbol{S}_\mathrm{f},\boldsymbol{\xi}) = -Q_3(\boldsymbol{S}_\mathrm{f},-\boldsymbol{\xi})$. The Stokes parameters $\boldsymbol{\xi}$ is set to be $\pm(\boldsymbol{Q}_2+\boldsymbol{q}_3)/|\boldsymbol{Q}_2+\boldsymbol{q}_3|$, with relative probabilities

$$P_{++}\left(\boldsymbol{S}_\mathrm{f}=\frac{\boldsymbol{Q}_1}{|\boldsymbol{Q}_1|},\boldsymbol{\xi}=\frac{\boldsymbol{Q}_2+\boldsymbol{q}_3}{|\boldsymbol{Q}_2+\boldsymbol{q}_3|}\right)=\frac{Q_0+|\boldsymbol{Q}_1|}{2Q_0}\times\frac{Q_0+|\boldsymbol{Q}_1|+|\boldsymbol{Q}_2+\boldsymbol{q}_3|}{2(Q_0+|\boldsymbol{Q}_1|)}, \tag{B.5}$$

$$P_{+-}\left(\boldsymbol{S}_\mathrm{f}=\frac{\boldsymbol{Q}_1}{|\boldsymbol{Q}_1|},\boldsymbol{\xi}=-\frac{\boldsymbol{Q}_2+\boldsymbol{q}_3}{|\boldsymbol{Q}_2+\boldsymbol{q}_3|}\right)=\frac{Q_0+|\boldsymbol{Q}_1|}{2Q_0}\times\frac{Q_0+|\boldsymbol{Q}_1|-|\boldsymbol{Q}_2+\boldsymbol{q}_3|}{2(Q_0+|\boldsymbol{Q}_1|)}, \tag{B.6}$$

$$P_{-+}\left(\boldsymbol{S}_\mathrm{f}=-\frac{\boldsymbol{Q}_1}{|\boldsymbol{Q}_1|},\boldsymbol{\xi}=\frac{\boldsymbol{Q}_2-\boldsymbol{q}_3}{|\boldsymbol{Q}_2-\boldsymbol{q}_3|}\right)=\frac{Q_0-|\boldsymbol{Q}_1|}{2Q_0}\times\frac{Q_0-|\boldsymbol{Q}_1|+|\boldsymbol{Q}_2-\boldsymbol{q}_3|}{2(Q_0-|\boldsymbol{Q}_1|)}, \tag{B.7}$$

$$P_{--}\left(\boldsymbol{S}_\mathrm{f}=-\frac{\boldsymbol{Q}_1}{|\boldsymbol{Q}_1|},\boldsymbol{\xi}=-\frac{\boldsymbol{Q}_2-\boldsymbol{q}_3}{|\boldsymbol{Q}_2-\boldsymbol{q}_3|}\right)=\frac{Q_0-|\boldsymbol{Q}_1|}{2Q_0}\times\frac{Q_0-|\boldsymbol{Q}_1|-|\boldsymbol{Q}_2-\boldsymbol{q}_3|}{2(Q_0-|\boldsymbol{Q}_1|)}, \tag{B.8}$$

where $\boldsymbol{q}_3$ is the mean vector of $Q_3(\boldsymbol{S}_\mathrm{f},\boldsymbol{\xi})$ with respect to $\boldsymbol{\xi}$. Accordingly, the average vector $\overline{\boldsymbol{\xi}}$ is along

$$\overline{\boldsymbol{\xi}}^*=\frac{\boldsymbol{Q}_2+\boldsymbol{q}_3}{|\boldsymbol{Q}_2+\boldsymbol{q}_3|}P_{++}-\frac{\boldsymbol{Q}_2+\boldsymbol{q}_3}{|\boldsymbol{Q}_2+\boldsymbol{q}_3|}P_{+-}+\frac{\boldsymbol{Q}_2-\boldsymbol{q}_3}{|\boldsymbol{Q}_2-\boldsymbol{q}_3|}P_{-+}-\frac{\boldsymbol{Q}_2-\boldsymbol{q}_3}{|\boldsymbol{Q}_2-\boldsymbol{q}_3|}P_{--}=\frac{\boldsymbol{Q}_2}{Q_0}. \tag{B.9}$$

Equations (B.4) and (B.9) suggest that the average vectors $\overline{\boldsymbol{\xi}}$ and $\overline{\boldsymbol{S}}_\mathrm{f}$ via calculating $\boldsymbol{S}_\mathrm{f}$ first and then $\boldsymbol{\xi}$ are independent of $Q_3(\boldsymbol{S}_\mathrm{f},\boldsymbol{\xi})$, which are the same as those via calculating them separately. Similarly, the identical results can be obtained by calculating $\boldsymbol{\xi}$ first and then $\boldsymbol{S}_\mathrm{f}$; however, in practice this determination order is very challenging, since $Q_3(\boldsymbol{S}_\mathrm{f},\boldsymbol{\xi})$ cannot be written in the form of $\boldsymbol{S}_\mathrm{f}\cdot\boldsymbol{q}_3'(\boldsymbol{\xi})$, which greatly increase the difficulty for knowing its mean vector $\boldsymbol{q}_3'$ with respect to $\boldsymbol{S}_\mathrm{f}$. We conclude that it is favorable for determining $\boldsymbol{S}_\mathrm{f}$ and $\boldsymbol{\xi}$ separately to avoid computing the complex correlation term, as we performed in this work.

ORCID iDs

Huai-Hang Song https://orcid.org/0000-0002-2587-4658
Wei-Min Wang https://orcid.org/0000-0002-9852-1589
Yan-Fei Li https://orcid.org/0000-0003-2832-275X

References

[1] Cartlidge E 2018 *Science* **359** 382
[2] Danson C N *et al* 2019 *High Power Laser Sci. Eng.* **7** e54
[3] Strickland D and Mourou G 1985 *Opt. Commun.* **56** 219
[4] Sung J H *et al* 2017 *Opt. Lett.* **42** 2058
[5] Tanaka K A *et al* 2020 *Matter Radiat. Extremes* **5** 024402
[6] Lureau F *et al* 2020 *High Power Laser Sci. Eng.* **8** e43
[7] Di Piazza A, Müller C, Hatsagortsyan K Z and Keitel C H 2012 *Rev. Mod. Phys.* **84** 1177
[8] Mourou G 2019 *Rev. Mod. Phys.* **91** 030501
[9] Blackburn T G 2020 *Rev. Mod. Plasma Phys.* **4** 5
[10] Ritus V I 1985 *J. Russ. Laser Res.* **6** 497
[11] Berestetskii V B, Lifshitz E M and Pitaevskii L P 1982 *Quantum Electrodynamics* (Oxford: Heinemann)
[12] Baier V N, Katkov V and Strakhovenko V M 1998 *Electromagnetic Processes at High Energies in Oriented Single Crystals* (Singapore: World Scientific)
[13] Reiss H R 1962 *J. Math. Phys.* **3** 59
[14] Burke D L *et al* 1997 *Phys. Rev. Lett.* **79** 1626
[15] Sokolov I V, Naumova N M, Nees J A and Mourou G A 2010 *Phys. Rev. Lett.* **105** 195005
[16] Blackburn T G, Ilderton A, Murphy C D and Marklund M 2017 *Phys. Rev.* A **96** 022128
[17] Bell A R and Kirk J G 2008 *Phys. Rev. Lett.* **101** 200403
[18] Nerush E N *et al* 2011 *Phys. Rev. Lett.* **106** 035001
[19] Grismayer T, Vranic M, Martins J L, Fonseca R A and Silva L O 2017 *Phys. Rev.* E **95** 023210
[20] Zhu X-L *et al* 2016 *Nat. Commun.* **7** 13686
[21] Ridgers C P *et al* 2012 *Phys. Rev. Lett.* **108** 165006
[22] Kostyukov I Y and Nerush E N 2016 *Phys. Plasmas* **23** 093119
[23] Del Sorbo D *et al* 2018 *New J. Phys.* **20** 033014
[24] Wang W-M, Gibbon P, Sheng Z-M, Li Y-T and Zhang J 2017 *Phys. Rev.* E **96** 013201
[25] Goldreich P and Julian W H 1969 *Astrophys. J.* **157** 869
[26] Piran T 2005 *Rev. Mod. Phys.* **76** 1143
[27] Lobet M, Ruyer C, Debayle A, d'Humières E, Grech M, Lemoine M and Gremillet L 2015 *Phys. Rev. Lett.* **115** 215003
[28] Ruffini R, Vereshchagin G and Xue S-S 2010 *Phys. Rep.* **487** 1
[29] Danielson J R, Dubin D H E, Greaves R G and Surko C M 2015 *Rev. Mod. Phys.* **87** 247
[30] King B, Elkina N and Ruhl H 2013 *Phys. Rev.* A **87** 042117
[31] Büscher M, Hützen A, Ji L and Lehrach A 2020 *High Power Laser Sci. Eng.* **8** e36
[32] Seipt D and King B 2020 *Phys. Rev.* A **102** 052805
[33] Li Y-F, Shaisultanov R, Hatsagortsyan K Z, Wan F, Keitel C H and Li J-X 2019 *Phys. Rev. Lett.* **122** 154801
[34] Song H-H, Wang W-M, Li J-X, Li Y-F and Li Y-T 2019 *Phys. Rev.* A **100** 033407
[35] Seipt D, Del Sorbo D, Ridgers C P and Thomas A G R 2019 *Phys. Rev.* A **100** 061402
[36] Sokolov A A and Ternov I M 1968 *Synchrotron Radiation* (New York: Academic)
[37] Baier V N and Katkov V M 1967 *Phys. Lett.* A **24** 327
[38] Wan F, Shaisultanov R, Li Y-F, Hatsagortsyan K Z, Keitel C H and Li J-X 2020 *Phys. Lett.* B **800** 135120
[39] Chen Y-Y, He P-L, Shaisultanov R, Hatsagortsyan K Z and Keitel C H 2019 *Phys. Rev. Lett.* **123** 174801
[40] Li Y-F, Chen Y-Y, Wang W-M and Hu H-S 2020 *Phys. Rev. Lett.* **125** 044802
[41] King B and Elkina N 2016 *Phys. Rev.* A **94** 062102
[42] Li Y-F, Shaisultanov R, Chen Y-Y, Wan F, Hatsagortsyan K Z, Keitel C H and Li J-X 2020 *Phys. Rev. Lett.* **124** 014801
[43] Xue K *et al* 2020 *Matter Radiat. Extremes* **5** 054402
[44] Wan F *et al* 2020 *Phys. Rev. Res.* **2** 032049
[45] Seipt D, Ridgers C P, Del Sorbo D and Thomas A G R 2021 *New J. Phys.* **23** 053025
[46] Jirka M *et al* 2016 *Phys. Rev.* E **93** 023207
[47] Ridgers C P, Kirk J G, Duclous R, Blackburn T G, Brady C S, Bennett K, Arber T D and Bell A R 2014 *J. Comput. Phys.* **260** 273
[48] Yokoya K 2011 *User's Manual of CAIN* version 2.42
[49] McMaster W H 1961 *Rev. Mod. Phys.* **33** 8
[50] Di Piazza A, Tamburini M, Meuren S and Keitel C H 2018 *Phys. Rev.* A **98** 012134
[51] Ilderton A, King B and Seipt D 2019 *Phys. Rev.* A **99** 042121
[52] Elkina N V *et al* 2011 *Phys. Rev. Spec. Top. Accel. Beams* **14** 054401
[53] Green D G and Harvey C N 2015 *Comput. Phys. Commun.* **192** 313
[54] Gonoskov A *et al* 2015 *Phys. Rev.* E **92** 023305
[55] Bargmann V, Michel L and Telegdi V L 1959 *Phys. Rev. Lett.* **2** 435
[56] Baier V N 1972 *Sov. Phys. Usp.* **14** 695
[57] Song H-H, Wang W-M and Li Y-T 2021 arXiv:2104.00642
[58] Esirkepov T Z, Bulanov S S, Koga J K, Kando M, Kondo K, Rosanov N N, Korn G and Bulanov S V 2015 *Phys. Lett.* A **379** 2044